

# Pairing in spherical nuclei: quasi-particle random phase approximation calculations with the Gogny interaction

V. De Donno

*Dipartimento di Matematica e Fisica “E. De Giorgi”, Università del Salento, I-73100 Lecce, ITALY*

G. Co’

*Dipartimento di Matematica e Fisica “E. De Giorgi”,  
Università del Salento, I-73100 Lecce, ITALY and,  
INFN Sezione di Lecce, Via Arnesano, I-73100 Lecce, ITALY*

M. Anguiano, A. M. Lallena

*Departamento de Física Atómica, Molecular y Nuclear,  
Universidad de Granada, E-18071 Granada, SPAIN*

(Dated: May 23, 2017)

We investigate the effects of the pairing in spherical nuclei. We use the same finite-range interaction of Gogny type in the three steps of our approach, Hartree-Fock, Bardeen, Cooper and Schrieffer, and quasi-particle random phase approximation calculations. We study electric and magnetic dipole, quadrupole and octupole excitations in oxygen and calcium isotopes and also in isotones with 20 neutrons. We investigate the pairing effects on single particle energies and occupation probabilities, on the excitation energies,  $B$ -values and collectivity of low-lying states including the isoscalar electric dipole and the magnetic dipole excitations, and also the giant resonances. The inclusion of the pairing increases the values of the excitation energies in all the cases we have studied. In general, the effects of the pairing are too small to remarkably improve the agreement with the available experimental data.

PACS numbers: 21.60.Jz; 25.40.Kv

## I. INTRODUCTION

In atomic nuclei, pairing is the most striking phenomenon whose description requires an extension of the extreme mean-field model. For example, the evidence that the angular momentum of each even-even nucleus is zero, without any exception, and that the angular momentum of each odd-even nucleus coincides with that of the single particle (s.p.) level occupied by the unpaired nucleon can be explained only by assuming the presence between like-nucleons of an attractive two-body interaction, therefore, by definition, not described by the one-body mean-field potential.

Pairing phenomena have been described by extending to the nuclear case the theory of Bardeen, Cooper and Schrieffer (BCS) originally formulated to study superconductivity in metals [1]. The BCS theory requires two inputs, the s.p. energies and wave functions, in our case generated by Hartree-Fock (HF) calculations, and the pairing interaction. This theory, usually applied to describe the ground state properties of even-even open shell nuclei, provides the occupation probabilities of the s.p. levels, and the quasi-particle energies. An analogous description of open shell nuclei is also given by the Hartree-Fock-Bogoliubov (HFB) theory which is formulated to use a single input, the effective nucleon-nucleon interaction, to generate s.p. wave functions, occupation probabilities, and quasi-particle energies.

The description of the excited states requires to go beyond the HF+BCS or the HFB frameworks which are, both, unable to consider collective effects. For this reason an extension of the Random Phase Approximation (RPA) theory, called quasi-particle RPA (QRPA) [2], built to handle pairing and partial occupation probabilities of the s.p. levels, is commonly used.

In these last few years we have developed a model which treats the pairing by using a set of s.p. levels generated by a HF calculation [3–5]. In this approach we use the same finite-range interaction as nucleon-nucleon force in the HF calculations and also as a pairing force in the BCS approach. In the works quoted above we tested our results against those obtained in HFB calculations, and we found good agreement between the two approaches. Specifically, the two types of calculations agree very well for those quantities which are used in QRPA calculations, i.e. occupation probabilities and quasi-particle energies.

Encouraged by this result we constructed a QRPA on top of our HF+BCS approach by using the same finite-range interaction. We have now the possibility of describing ground and excited states of spherical open-shell nuclei by using an approach which requires a single input, the nucleon-nucleon finite-range interaction. As already pointed out in the seminal paper of Dechargé and Gogny [6], the use of finite-range interaction provides stability of the pairing results against the size of the s.p. configuration space. For this reason, once the nucleon-nucleon interaction has been chosen, our calculations do not require any other input parameter related to the physics of the problem.

In the literature one can find various types of QRPA calculations, as indicated, for example, by the review article of Ref. [7]. Without the ambition of being exhaustive in quoting the works done in this field, we classify them in three categories. There are calculations where the s.p. wave functions and energies are generated by a mean-field potential, for example of Woods-Saxon or harmonic oscillator type. The BCS equations are solved by using a phenomenological pairing interaction whose parameters are selected to reproduce some properties of the nuclei investigated. Usually, the same pairing interaction is also used in QRPA calculations. In other types of calculations the interaction used in the HF procedure is different from that used to evaluate the pairing. These are, for example, the calculations carried out with the Skyrme interaction [8–12] whose zero-range character does not allow its straightforward use in the pairing sector since the results strongly depend on the size of the quasi-particle configuration space [6]. The last type of calculations use the same interaction to generate s.p. levels, pairing and QRPA excitations. Our calculations, as well as those of Refs. [13, 14], belong to this last category. There are also calculations carried out within the relativistic framework that can be classified in an analogous way (see for example [15, 16].)

In the present paper we use our HF+BCS+QRPA approach to investigate the relevance of the pairing in the different steps of the calculations. By switching on and off the various terms of our equations we disentangle the pairing effects in the s.p. energies and occupation probabilities, from those related to the QRPA approach.

Our article is structured as follows. In Sec. II we describe HF+BCS and QRPA approach. The technical details of the calculations are given in Sec. III. In Sec. IV we show the results obtained by using the D1M Gogny interaction [17]. Our calculations have been carried out for a set of oxygen and calcium isotopes and an isotone chain composed by nuclei with 20 neutrons. We discuss results concerning positive and negative parity multipoles excitations from the dipole to the octupole excitations. We analyze the pairing effects first on the low-lying excitations and, later, on the giant resonances. The conclusions of our study are presented in Sec. V. Finally, in the Appendix A a detailed set of results regarding the  $^{18}\text{O}$  nucleus is presented, in order to discuss in detail the numerical convergence of our calculations.

## II. THE MODEL

The first step of our approach consists in the description of the nuclear ground state within the HF+BCS framework. We first generate a set of s.p. wave functions in a spherical basis by solving the HF equations. When the iterative method described in Ref. [18] has reached convergence, we calculate the direct, Hartree, and exchange, Fock-Dirac, potentials by using the s.p. wave functions below the Fermi level, and solve the integro-differential HF equations to generate the s.p. wave functions above it. Each s.p. state  $|\mu m_\mu\rangle \equiv |n_\mu l_\mu j_\mu m_\mu\rangle$  is characterized by the principal quantum number  $n_\mu$ , the orbital angular momentum  $l_\mu$ , the total angular momentum  $j_\mu$ , and its  $z$ -axis projection  $m_\mu$ , and has a s.p. energy  $\epsilon_\mu$  that is  $2j_\mu + 1$  times degenerated.

The HF wave functions and energies are used as the starting point to solve the BCS equations. From the solution of these equations, we obtain the Bogoliubov-Valatin  $v_\mu^2$  and  $u_\mu^2$  coefficients, which are normalized such that  $u_\mu^2 + v_\mu^2 = 1$ . The occupation probability of the  $|\mu\rangle$  s.p. state is  $v_\mu^2$ , while  $u_\mu^2$  is the probability of being empty. We consider only spherical nuclei, therefore the BCS ground states are spherically symmetric and the  $v_\mu$  and  $u_\mu$  coefficients are independent of  $m_\mu$ .

A quantity obtained in the BCS calculations and used in the QRPA is the quasi-particle energy, defined as

$$E_\mu \equiv \sqrt{(\epsilon_\mu - \lambda)^2 + \Delta_\mu^2}, \quad (1)$$

where  $\lambda$  is the chemical potential, which is calculated by using the expression

$$\lambda = \frac{\sum_\mu (2j_\mu + 1) \left( 2v_\mu^2 + \frac{\epsilon_\mu}{E_\mu} - 1 \right)}{\sum_\mu (2j_\mu + 1) \frac{1}{E_\mu}}, \quad (2)$$

and

$$\Delta_\mu = -\frac{1}{\sqrt{2j_\mu + 1}} \sum_\nu \sqrt{2j_\nu + 1} u_\nu v_\nu \langle \nu\nu; 0 | V | \mu\mu; 0 \rangle \quad (3)$$

where the expression  $|\alpha\beta; 0\rangle$  indicates the coupling of the  $|\alpha\rangle$  and  $|\beta\rangle$  s.p. states to the total angular momentum  $J = 0$ , and  $V$  represents the pairing interaction.

A QRPA excited state  $|k\rangle$  of angular momentum  $J$ , third component  $M$ , parity  $\Pi$ , and excitation energy  $\omega_k$ , is described as a combination of quasi-particle excitations on top of the ground state  $|0\rangle$ :

$$|k\rangle \equiv |J^\Pi M; \omega_k\rangle = \sum_{\mu \leq \mu'} \left[ X_{\mu\mu'}^{(k)}(J) A_{\mu\mu'}^\dagger(JM) + (-1)^{J+M+1} Y_{\mu\mu'}^{(k)}(J) A_{\mu\mu'}(J-M) \right] |0\rangle. \quad (4)$$

In the above expression, the condition  $\mu \leq \mu'$  prevents the double counting of the quasi-particle pairs. To simplify the writing we did not include the explicit dependence on the parity  $\Pi = (-1)^{l_\mu + l_{\mu'}}$ . The QRPA amplitudes  $X$  and  $Y$  must verify the relation [19, 20]

$$\sum_{\mu \leq \mu'} \left\{ [X_{\mu\mu'}^{(k)}(J)]^* X_{\mu\mu'}^{(k')}(J) - [Y_{\mu\mu'}^{(k)}(J)]^* Y_{\mu\mu'}^{(k')}(J) \right\} = \delta_{kk'} \quad (5)$$

obtained by imposing the orthonormality of the QRPA eigenstates, and by using the definition of the quasi-particle pair creation and annihilation operators

$$A_{\mu\mu'}^\dagger(JM) = C_{\mu\mu'}(J) \sum_{m_\mu, m_{\mu'}} \langle j_\mu m_\mu j_{\mu'} m_{\mu'} | J M \rangle \alpha_{\mu m_\mu}^\dagger \alpha_{\mu' m_{\mu'}}^\dagger \quad (6)$$

and

$$A_{\mu\mu'}(JM) = C_{\mu\mu'}(J) \sum_{m_\mu, m_{\mu'}} \langle j_\mu m_\mu j_{\mu'} m_{\mu'} | J M \rangle \alpha_{\mu m_\mu} \alpha_{\mu' m_{\mu'}} , \quad (7)$$

where

$$C_{\mu\mu'}(J) = \frac{\sqrt{1 + (-1)^J \delta_{\mu\mu'}}}{1 + \delta_{\mu\mu'}}. \quad (8)$$

The quasi-particle creation,  $\alpha_{\mu m_\mu}^\dagger$ , and annihilation,  $\alpha_{\mu m_\mu}$ , operators are related to the particle creation,  $c_{\mu m_\mu}^\dagger$ , and annihilation,  $c_{\mu m_\mu}$ , operators by means of the Bogoliubov-Valatin transformation [19, 20]

$$\alpha_{\mu \pm |m_\mu|}^\dagger = u_\mu c_{\mu \pm |m_\mu|}^\dagger \mp v_\mu c_{\mu \mp |m_\mu|}. \quad (9)$$

By using standard techniques the QRPA secular equations can be written as [19, 20]:

$$\begin{bmatrix} \mathcal{A}(J) & \mathcal{B}(J) \\ -\mathcal{B}^*(J) & -\mathcal{A}^*(J) \end{bmatrix} \begin{bmatrix} X^{(k)}(J) \\ Y^{(k)}(J) \end{bmatrix} = \omega_k \begin{bmatrix} X^{(k)}(J) \\ Y^{(k)}(J) \end{bmatrix}. \quad (10)$$

The matrix elements of  $\mathcal{A}$  and  $\mathcal{B}$  are given by the expressions:

$$\begin{aligned} \mathcal{A}_{[\mu\mu']J, [\nu\nu']J} &= (E_\mu + E_{\mu'}) \delta_{\mu\nu} \delta_{\mu'\nu'} \\ &+ C_{\mu\mu'}(J) C_{\nu\nu'}(J) \left\{ F(\mu\mu'\nu\nu'; J) (u_\mu \bar{v}_{\mu'} u_\nu \bar{v}_{\nu'} + \bar{v} \leftrightarrow u) \right. \\ &\quad - (-1)^{j_\nu + j_{\nu'} - J} F(\mu\mu'\nu'\nu; J) (u_\mu \bar{v}_{\mu'} \bar{v}_\nu u_{\nu'} + \bar{v} \leftrightarrow u) \\ &\quad \left. + G(\mu\mu'\nu\nu'; J) (u_\mu u_{\mu'} u_\nu u_{\nu'} + \bar{v} \leftrightarrow u) \right\} \end{aligned} \quad (11)$$

and

$$\begin{aligned} \mathcal{B}_{[\mu\mu']J, [\nu\nu']J} &= C_{\mu\mu'}(J) C_{\nu\nu'}(J) \left\{ F(\mu\mu'\nu\nu'; J) (u_\mu \bar{v}_{\mu'} \bar{v}_\nu u_{\nu'} + \bar{v} \leftrightarrow u) \right. \\ &\quad - (-1)^{j_\nu + j_{\nu'} - J} F(\mu\mu'\nu'\nu; J) (u_\mu \bar{v}_{\mu'} u_\nu \bar{v}_{\nu'} + \bar{v} \leftrightarrow u) \\ &\quad \left. - G(\mu\mu'\nu\nu'; J) (u_\mu u_{\mu'} \bar{v}_\nu \bar{v}_{\nu'} + \bar{v} \leftrightarrow u) \right\}. \end{aligned} \quad (12)$$

The secular QRPA equations are independent of the  $m$  quantum numbers because we are considering spherical nuclei. In the previous equations, in order to simplify the writing, we have introduced the symbol

$$\bar{v}_\mu = (-1)^\mu v_\mu. \quad (13)$$

On the other hand, the  $F$  and  $G$  functions in Eqs. (11) and (12) contain the matrix elements of the interaction; their expressions are:

$$F(\mu\mu'\nu\nu'; J) = \sum_K (-1)^{j'_\mu + j_\nu + K} (2K+1) \begin{Bmatrix} j_\mu & j_{\mu'} & J \\ j_\nu & j_{\nu'} & K \end{Bmatrix} \langle \mu\nu'; K | \bar{V} | \mu'\nu; K \rangle \quad (14)$$

and

$$G(\mu\mu'\nu\nu'; J) = \langle \mu\mu'; J | \bar{V} | \nu\nu'; J \rangle, \quad (15)$$

where

$$\langle \mu\nu'; J | \bar{V} | \mu'\nu; J \rangle = \langle \mu\nu'; J | V | \mu'\nu; J \rangle - \langle \mu\nu'; J | V | \nu\mu'; J \rangle \quad (16)$$

is the antisymmetrized interaction matrix element.

The transition amplitudes induced by an external operator  $Q_J^T$  are calculated by using the expression:

$$\begin{aligned} \langle J^\Pi; \omega_k | Q_J^T | 0 \rangle &= \sum_{\mu \leq \mu'} [u_\mu \bar{v}_{\mu'} + (-1)^J \bar{v}_\mu u_{\mu'}] \\ &\quad \left[ X_{\mu\mu'}^{(k)}(J) \langle \mu | Q_J^T | \mu' \rangle + (-1)^{J+j_\mu-j_{\mu'}} Y_{\mu\mu'}^{(k)}(J) \langle \mu' | Q_J^T | \mu \rangle \right], \end{aligned} \quad (17)$$

where the double bar indicates the reduced matrix element as defined by the Wigner-Eckart theorem [21].

In absence of pairing, Eqs. (11) and (12) do not reproduce the expressions of the usual RPA matrices [19, 20]. In this limit, the  $F$  terms (14) are the traditional transition matrix elements of the RPA. However, the  $G$  terms in Eq. (15), that do not have counterpart in the RPA equations, do not vanish, and they are simply decoupled from the  $F$  terms.

In BCS the number of the particles composing the system is conserved only on average. The QRPA theory is based on the BCS ground state, which is not an eigenstate of the particle number, and the corresponding solutions include terms related to nuclear systems with  $A \pm 2$  particles. A clear separation of these spurious components requires the use of projection techniques on the good number of particles (see for example [22–24]).

### III. DETAILS OF THE CALCULATIONS

Our formulation of the HF+BCS+QRPA equations can handle any local finite-range interaction that may, eventually, include density dependent terms. Among the various effective interactions available in the literature, we have chosen forces of Gogny type [25], which have been widely used and tested. We express the effective interaction as a sum of central,  $V_C$ , spin-orbit,  $V_{SO}$ , and density dependent,  $V_{DD}$ , terms:

$$V(1,2) = V_C(1,2) + V_{SO}(1,2) + V_{DD}(1,2). \quad (18)$$

The central term depends on the spin and the isospin of the two interacting nucleons and has a finite range, the other two terms are of zero-range type. In HF calculations, in addition to the force  $V$ , also the Coulomb interaction has been considered.

In the BCS calculations the spin-orbit,  $V_{SO}(1,2)$ , and the density-dependent,  $V_{DD}(1,2)$ , terms do not contribute, the former one because the interacting pair is coupled to zero angular momentum, and the latter one by construction in Gogny type interactions [25]. In our BCS calculations we use only the  $V_C$  term and we do not consider the Coulomb term. This is the approach commonly adopted in HFB calculations when Gogny type forces are used [6, 26, 27], and it is justified by the small effects produced by the Coulomb force. Specifically, for the nuclei we investigate in this article, we point out that there is no Coulomb interaction in the pairing sector for the oxygen and calcium isotopes where the pairing force is active only between neutrons. For the  $N = 20$  isotones we have evaluated the effect of the Coulomb force on the binding energies and we found relative differences between results with and without Coulomb forces of few parts on a thousand.

The QRPA calculations have been carried out by considering the complete Gogny interaction (18) plus the Coulomb force, even if we knew that the effects of the latter one and of the spin-orbit interaction are negligible [28].

In the next section we present the results obtained by using a parameterization of the Gogny interaction called D1M [17]. We have carried out our calculations also with the well known and widely used D1S parameterization [26]. We did not find significant differences between the results obtained with the two interactions in what refers to the pairing effects. Therefore, we show only the D1M results.

We solve the HF equations in  $r$ -space by imposing bound boundary conditions at the edge of the integration box [18, 29, 30]. In this manner all the s.p. states forming the configuration space are bound, even those with positive energy. The size of the s.p. configuration space is large enough to ensure the stability of the BCS results. The finite-range of the interactions automatically generates the convergence of the calculations without additional renormalisation parameters as it is required, for example, when Skyrme-like interactions are used [31]. In our BCS calculations we have considered all the s.p. states with energy up to 10 MeV. This configuration space, together with the Gogny interactions, provides the stability of the BCS ground-state energy within the keV range.

From the numerical point of view, the critical parameter in the QRPA calculations is the size of the s.p. configuration space which is strictly related to the dimension of the integration box. As already pointed out, in our calculations the continuum part of the s.p. spectrum is described in terms of bound wave functions with positive energy. The dimension of the integration box determines the s.p. energies and wave functions in the continuum. This procedure does not consider all the effects produced by a correct treatment of the continuum part of the s.p. configuration space. In Ref. [32] we have investigated these effects in RPA calculations. The effects in the pairing sector have been studied, for example in Ref. [33].

Our experience with continuum RPA calculations indicates that the observables we have investigated in the present work are scarcely sensitive to the exact treatment of the continuum s.p. spectrum. In analogy to what we have done in Ref. [28], we have chosen the sizes of the s.p. configuration spaces and the boxes dimensions by controlling that the centroid energies of the giant dipole resonances of closed shell nuclei do not change by more than 0.5 MeV when either the box size or the maximum value of the s.p. energy are increased. By using the values determined in this manner we obtain stability of our results. The number of the quasi-particle pairs depends on the size of the s.p. space and defines the dimensions of the QRPA secular matrix (10) to be diagonalized.

This choice of the configuration space sets below zero the spurious  $0^+$  excited state due to the breaking of the nucleon number conservation symmetry [10]. The case of the spurious  $1^-$  state due to the breaking of the translational invariance will be discussed in Sec. IV B. By using the  $^{18}\text{O}$  nucleus as test example, we give in Appendix A a more detailed presentation of our method to determine the size of the configuration space.

## IV. RESULTS

In this section we present a selection of the results of our calculations with the aim of studying the role of the pairing force in the excitation spectrum of spherical open shell nuclei as predicted by QRPA. Our investigation strategy consisted in switching on and off the pairing force in the various terms of the equations previously presented, therefore three different types of calculations have been carried out. In those labelled QRPA all the pairing terms are active, while we have switched off the  $G$  terms in Eqs. (11) and (12) in those calculations we have called QRPA(F). In both type of calculations the s.p. basis is that provided by the HF+BCS approach. This means that in QRPA(F) the pairing is present only in the s.p. input where energies, and occupation probabilities differ from those obtained in a pure HF calculation. In the third kind of calculation, which we call RPA, the s.p. input is provided by the HF, and the excited states are obtained by solving Eqs. (11) and (12) without the  $G$  terms. In this case, we indicate as  $(v_\mu^{\text{HF}})^2$  the occupation probability of the s.p. state  $|\mu\rangle$ . Its value is 1 or 0 except for the only partially occupied s.p. state in each one of the open-shell nuclei investigated.

In this article, we present the results obtained for 6 oxygen isotopes, from  $A = 16$  up to  $A = 26$ , 12 calcium isotopes, from  $A = 40$  up to  $A = 62$ , and a chain of 9 isotones with  $N = 20$ , from  $^{30}\text{Ne}$  to  $^{46}\text{Fe}$ . All the nuclei we have considered are spherical, magic or semi-magic.

### A. Single particle energies and occupation probabilities

We have already discussed in other publications the effect of the pairing on the ground-state properties of spherical semi-magic nuclei, which we describe with our HF+BCS approach [3–5]. Here we address our attention on how the pairing modifies the occupation numbers and the energies of the s.p. states that are input of the QRPA calculations. For this purpose we have considered the quantities

$$\delta v_\mu = |v_\mu^2 - (v_\mu^{\text{HF}})^2| \quad (19)$$

and

$$\delta\epsilon_\mu = \left| \frac{\tilde{\epsilon}_\mu - \epsilon_\mu}{\tilde{\epsilon}_\mu + \epsilon_\mu} \right|, \quad (20)$$

where, in analogy with the HF s.p. energies  $\epsilon_\mu$ , we have introduced the BCS s.p. energies  $\tilde{\epsilon}_\mu$  defined as

$$\tilde{\epsilon}_\mu = \pm E_\mu + \lambda, \quad (21)$$

with  $E_\mu$  indicating the quasi-particle energy defined in Eq. (1). Here the plus sign is taken for s.p. states where  $\epsilon_\mu > \lambda$ , while the minus sign corresponds to those s.p. states with  $\epsilon_\mu < \lambda$ .

We have found that the values  $\delta v_\mu$  and  $\delta\epsilon_\mu$  obtained for each individual nucleus are completely uncorrelated, with Pearson correlation coefficients well below 0.1 in all cases. The same happens for

$$\Delta v = \sum_\mu \delta v_\mu \quad (22)$$

and

$$\Delta\epsilon = \sum_\mu \delta\epsilon_\mu \quad (23)$$

calculated for each of the nuclei analyzed. For these quantities, the Pearson correlation coefficient is smaller than 0.04. This scarce correlation is evident in Fig. 1 where we show the values  $\Delta v$  and  $\Delta\epsilon$  for all the nuclei we have investigated. The zeros in both panels of the figure indicate the closed-shell nuclei, which are  $^{16}\text{O}$  and  $^{24}\text{O}$  for  $Z = 8$ ,  $^{40}\text{Ca}$ ,  $^{48}\text{Ca}$ ,  $^{52}\text{Ca}$ , and  $^{60}\text{Ca}$  for  $Z = 20$  and  $^{34}\text{Si}$  and, again,  $^{40}\text{Ca}$  for  $N = 20$ . In these nuclei the pairing is irrelevant, the s.p. states are fully occupied, or completely empty, and  $\tilde{\epsilon}_\mu \sim \epsilon_\mu$ . A clear example of the poor correlation between  $\Delta v$  and  $\Delta\epsilon$  is the case of the  $^{22}\text{O}$  nucleus where  $\Delta v$  shows the largest value of the isotope chain while that of  $\Delta\epsilon$  is the smallest one of the semi-magic nuclei considered. The contrary happens in  $^{26}\text{O}$ .

In panel (a) we notice that the effects of the pairing on  $\Delta v$  are similar in all the nuclei studied except in  $^{54}\text{Ca}$ ,  $^{56}\text{Ca}$ ,  $^{36}\text{S}$  and  $^{38}\text{Ar}$  where they are notably larger. This is due to the fact that in these nuclei the HF energy gaps between the last occupied and the first (partially) unoccupied s.p. state are small and this makes the pairing to be more relevant.

In Table I we present, for these four nuclei, the HF and BCS occupation probabilities and energies for those s.p. states with  $v_\mu^2 > 10^{-3}$ . The table shows that  $\tilde{\epsilon}_\mu < \epsilon_\mu$  for those quasi-particle states where  $\epsilon_\mu < \lambda$ , while the contrary happens if  $\epsilon_\mu > \lambda$ . This is a consequence of the definition of the quasi-particle energy  $E_\mu$ , see Eq. (1), where the pairing contribution  $\Delta_\mu$  is present in quadratic form. For this reason, the inclusion of the pairing always increases the  $E_\mu + E_{\mu'}$  factor of the  $\mathcal{A}$  term of the QRPA secular equation (11).

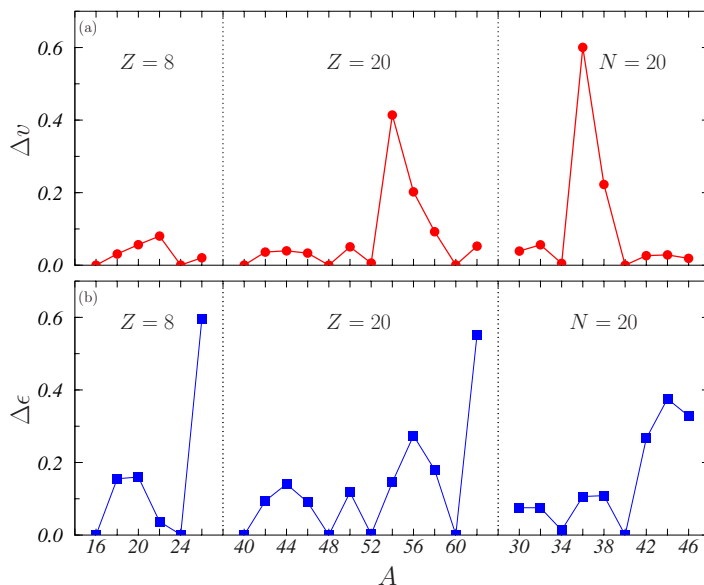


Figure 1: Values of (a)  $\Delta v$  and (b)  $\Delta\epsilon$ , defined in Eqs. (22) and (23), respectively, for the nuclei studied.



	<sup>36</sup> S ( $\lambda = -10.95$ MeV)				<sup>38</sup> Ar ( $\lambda = -9.24$ MeV)				<sup>54</sup> Ca ( $\lambda = -3.14$ MeV)				<sup>56</sup> Ca ( $\lambda = -2.82$ MeV)			
$\mu$	$(v_{\mu}^{\text{HF}})^2$	$v_{\mu}^2$	$\epsilon_{\mu}$	$\tilde{\epsilon}_{\mu}$	$(v_{\mu}^{\text{HF}})^2$	$v_{\mu}^2$	$\epsilon_{\mu}$	$\tilde{\epsilon}_{\mu}$	$(v_{\mu}^{\text{HF}})^2$	$v_{\mu}^2$	$\epsilon_{\mu}$	$\tilde{\epsilon}_{\mu}$	$(v_{\mu}^{\text{HF}})^2$	$v_{\mu}^2$	$\epsilon_{\mu}$	$\tilde{\epsilon}_{\mu}$
$1s_{1/2}$	1.000	0.999	-44.71	-44.76	1.000	0.999	-42.83	-42.87	1.000	1.000	-49.22	-49.23	1.000	1.000	-48.45	-48.47
$1p_{3/2}$	1.000	0.999	-30.70	-30.76	1.000	0.999	-29.23	-29.28	1.000	1.000	-36.07	-36.08	1.000	1.000	-35.60	-35.62
$1p_{1/2}$	1.000	0.998	-27.04	-27.12	1.000	0.997	-25.38	-25.46	1.000	1.000	-32.53	-32.55	1.000	0.999	-32.31	-32.34
$1d_{5/2}$	1.000	0.990	-17.01	-17.13	1.000	0.992	-16.08	-16.19	1.000	1.000	-22.52	-22.54	1.000	0.999	-22.42	-22.45
$2s_{1/2}$	1.000	0.618	-11.30	-12.42	1.000	0.867	-10.59	-11.08	1.000	0.999	-17.15	-17.18	1.000	0.999	-17.34	-17.38
$1d_{3/2}$	0.000	0.200	-10.00	-9.37	0.500	0.570	-9.43	-10.60	1.000	0.999	-16.82	-16.85	1.000	0.998	-16.62	-16.68
$1f_{7/2}$	0.000	0.003	-2.96	-2.90	0.000	0.005	-2.51	-2.44	1.000	0.997	-10.07	-10.11	1.000	0.995	-10.28	-10.35
$2p_{3/2}$	0.000	0.001	0.99	1.00	0.000	0.001	1.69	1.71	1.000	0.984	-5.85	-5.94	1.000	0.985	-6.02	-6.12
$2p_{1/2}$									1.000	0.717	-3.46	-3.89	1.000	0.878	-3.72	-4.00
$1f_{5/2}$	0.000	0.001	4.35	4.37	0.000	0.001	5.15	5.17	0.000	0.104	-2.15	-1.89	0.333	0.378	-2.56	-1.73
$1g_{9/2}$									0.000	0.003	1.92	1.95	0.000	0.008	1.45	1.52

Table I: Occupation probabilities,  $(v_{\mu}^{\text{HF}})^2$  and  $v_{\mu}^2$ , and s.p. energies,  $\epsilon_{\mu}$  and  $\tilde{\epsilon}_{\mu}$ , expressed in MeV, for the four nuclei showing the largest  $\Delta v$  values in Fig. 1. The s.p. states indicated are proton states for <sup>36</sup>S and <sup>38</sup>Ar, and neutron states for <sup>54</sup>Ca and <sup>56</sup>Ca.

The relatively large values of  $\Delta\epsilon$  for the <sup>26</sup>O and <sup>62</sup>Ca nuclei shown in the panel (b) of Fig. 1 are generated by the smallness of the denominator in Eq. (20). In these nuclei, the s.p. energies of the partially occupied  $(1d_{3/2})_{\nu}$  and  $(1g_{9/2})_{\nu}$  are close to 0, in absolute value, in both HF and HF+BCS cases, therefore, the values of the denominators of the  $\delta\epsilon_{\mu}$  factors become comparatively smaller than those of the other nuclei.

## B. Excited state energies

After having clarified the effect of the pairing on the input of our calculations, we present now the QRPA results. We first discuss the low-lying excitations. We show in Fig. 2 the excitation energies,  $\omega$ , of the main  $1^{-}$ ,  $2^{+}$  and  $3^{-}$  excited states below the giant resonance region obtained in the RPA calculations for the nuclei we have considered. Similar calculations have been carried out for  $1^{+}$ ,  $2^{-}$  and  $3^{+}$  excitations. In the figure, the horizontal black lines represent the RPA results, while the solid circles and the triangles are those obtained in QRPA(F) and QRPA calculations, respectively. In Fig. 2(c), the open squares indicate the experimental energies of some  $3^{-}$  excitations taken from Ref. [34].

In the upper panel of Fig. 2, where the  $1^{-}$  results are shown, all the nuclei present a first low-lying excitation at about 2 – 3 MeV. This is a spurious state generated by the breaking of the translational invariance of the QRPA equations [19]. The presence of this state in the excitation spectrum is strictly related to the use of a discretized and truncated quasi-particle configuration space. As we have tested in RPA calculations, which have analogous problems, a proper treatment of the continuum s.p. space set to zero this state [32]. For the purposes of the present work, since this state is easily identifiable and well isolated from the other ones, we have eliminated it by hand as it has been done in Ref. [35], and in the following discussion is not considered. A more detailed discussion about the presence of the spurious state is done in the appendix A.

The first observation about Fig. 2 is that the differences between the results generated by the various terms containing the pairing force are relatively small as compared to the values of the corresponding excitation energies. To have a clearer view of these energy differences we show in Fig. 3  $\omega_{\text{QRPA(F)}} - \omega_{\text{RPA}}$  (solid circles) and  $\omega_{\text{QRPA}} - \omega_{\text{RPA}}$  (triangles) for the same three multipolarities. It is evident that in the great majority of the cases considered, the QRPA(F) and QRPA excitation energies are larger than the energies obtained in RPA calculations. This is, mainly, a consequence of the increase of  $E_{\mu} + E_{\mu'}$ , previously discussed.

A more compact information about this result is given in Table II where we show, for each of the excitation multipoles studied, the average values of the differences shown in Fig. 3. In this table, also the results obtained for the unnatural parity excitations  $1^{+}$ ,  $2^{-}$  and  $3^{+}$  are given. All the average values of  $\omega_{\text{QRPA(F)}} - \omega_{\text{RPA}}$  and  $\omega_{\text{QRPA}} - \omega_{\text{RPA}}$  are positive. As seen in Fig. 3 we have found maximum differences of about 2 MeV for  $1^{-}$ , 3 MeV for  $2^{+}$  and 1.5 MeV for  $3^{-}$ , while the averages are 1 MeV at most. The table shows that the values of the standard deviations are rather large, comparable with the values of the averages.

Since the s.p. input in QRPA and QRPA(F) calculations is the same, the differences between the energies  $\omega_{\text{QRPA}}$  and  $\omega_{\text{QRPA(F)}}$  are only due to the presence of the pairing force in the  $G$  terms of the QRPA. The results of Figs. 2 and 3 indicate that, in general,  $\omega_{\text{QRPA(F)}}$  is larger than  $\omega_{\text{QRPA}}$ . The average values of the differences  $\omega_{\text{QRPA}} - \omega_{\text{QRPA(F)}}$  given in Table II summarize this result. These values are all negative and remarkably smaller than the respective mean

of the differences with the RPA energies. The s.p. input containing the pairing, HF+BCS, enhances the excitation energy values, but the presence of the pairing in the QRPA calculations slightly reduces this effect.

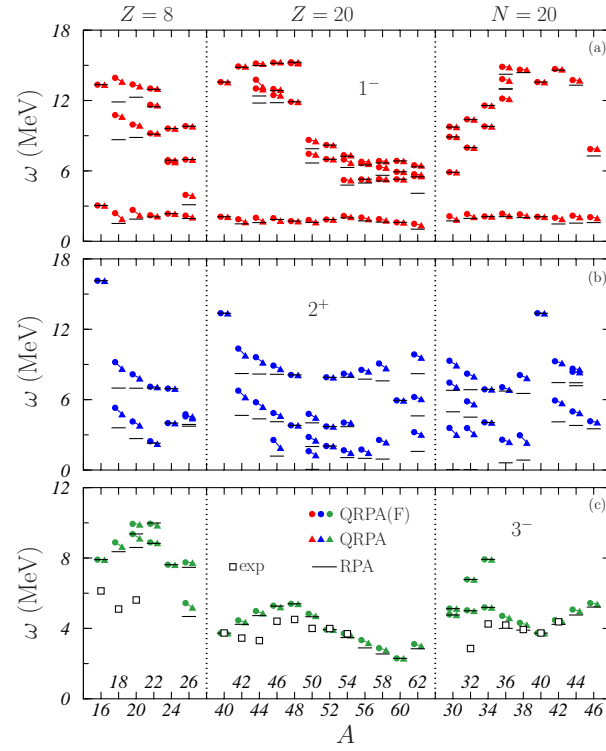


Figure 2: Excitation energies of the (a)  $1^-$ , (b)  $2^+$ , and (c)  $3^-$  states for all the nuclei under investigation. The black horizontal lines indicate the RPA results, and the circles and triangles those obtained in QRPA(F) and QRPA calculations, respectively. The open squares in panel (c) represent the experimental data taken from Ref. [34].

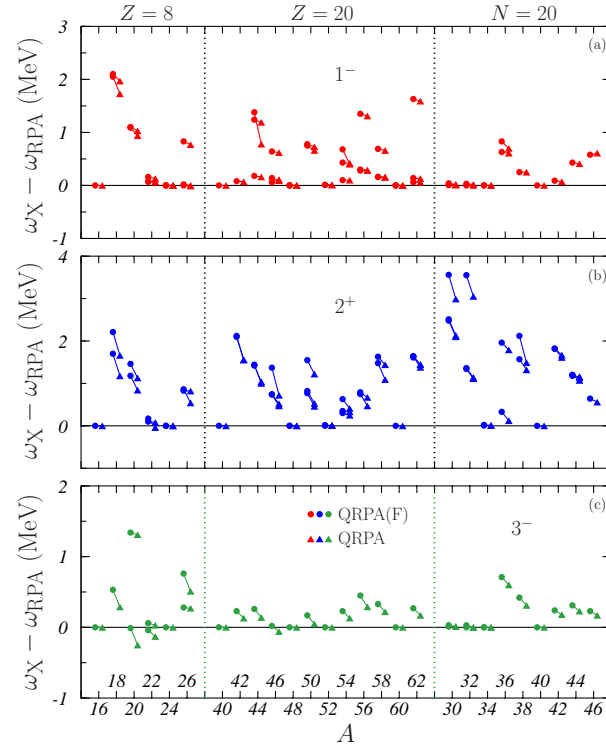


Figure 3: Differences between the excitation energies obtained in QRPA(F) (circles) and QRPA (triangles) and those found in RPA calculations, for the  $1^-$ , panel (a),  $2^+$ , panel (b), and  $3^-$ , panel (c), excited states.



state	$\omega_{\text{QRPA(F)}} - \omega_{\text{RPA}}$		$\omega_{\text{QRPA}} - \omega_{\text{RPA}}$		$\omega_{\text{QRPA}} - \omega_{\text{QRPA(F)}}$	
	av.	s.d.	av.	s.d.	av.	s.d.
$1^-$	0.35	0.39	0.31	0.35	0.00	0.20
$2^+$	1.07	0.63	0.85	0.53	-0.22	0.47
$3^-$	0.21	0.21	0.14	0.19	-0.07	0.07
$1^+$	0.81	0.54	0.90	0.60	-0.08	0.58
$2^-$	0.30	0.27	0.26	0.24	-0.05	0.17
$3^+$	0.72	0.54	0.69	0.52	-0.03	0.47

Table II: Averages (av.) and standard deviations (s.d.) of the energy differences shown in Fig. 3, and also of those obtained for the  $1^+$ ,  $2^-$  and  $3^+$  multipole excitations. All the quantities are expressed in MeV.

It is also worth remarking that the average energy differences, as well as the corresponding standard deviations, shown in Table II, are three times larger for positive parity excitations than for the negative ones. This is due to the fact that, in the first case, the transitions between spin-orbit partner levels are allowed. As some of these partner states are close to the Fermi surface, the pairing produces relatively large effects.

		$\mathcal{W}(\mu\mu'; J^\Pi)$							
		$2^+$				$2^-$			
A	configuration	RPA	QRPA(F)	QRPA	configuration	RPA	QRPA(F)	QRPA	
Z = 8	16				$(1d_{5/2}, 1p_{1/2})_\nu$	0.531	0.531	0.531	
	18	$(2s_{1/2}, 1d_{5/2})_\nu$	0.989	0.952	0.881	$(1d_{5/2}, 1p_{1/2})_\nu$	0.528	0.797	0.752
	20	$(2s_{1/2}, 1d_{5/2})_\nu$	0.972	0.727	0.766	$(1d_{5/2}, 1p_{1/2})_\nu$	0.553	0.945	0.760
	22	$(2s_{1/2}, 1d_{5/2})_\nu$	0.954	0.937	0.685				
	24	$(1d_{3/2}, 2s_{1/2})_\nu$	0.994	0.994	0.994				
	26	$(1d_{3/2}, 2s_{1/2})_\nu$	0.921	0.937	0.772	$(2p_{3/2}, 1d_{3/2})_\nu$	0.996	0.996	0.998
Z = 20	40				$(1f_{7/2}, 1d_{3/2})_\nu$	0.520	0.520	0.520	
	42	$(2p_{3/2}, 1f_{7/2})_\nu$	0.980	0.974	0.952	$(1f_{7/2}, 1d_{3/2})_\nu$	0.567	0.768	0.736
	44	$(2p_{3/2}, 1f_{7/2})_\nu$	0.979	0.944	0.921	$(1f_{7/2}, 1d_{3/2})_\nu$	0.615	0.902	0.867
	46	$(2p_{3/2}, 1f_{7/2})_\nu$	0.938	0.901	0.901	$(1f_{7/2}, 1d_{3/2})_\nu$	0.937	0.962	0.945
	48	$(2p_{3/2}, 1f_{7/2})_\nu$	0.936	0.936	0.936				
	50	$(2p_{3/2}, 1f_{7/2})_\nu$	0.940	0.902	0.756				
	50	$(2p_{1/2}, 2p_{3/2})_\nu$	0.986	0.960	0.926				
	52	$(2p_{1/2}, 2p_{3/2})_\nu$	0.984	0.984	0.978				
	54	$(1f_{5/2}, 2p_{1/2})_\nu$	0.991	0.917	0.772				
	56	$(1f_{5/2}, 2p_{1/2})_\nu$	0.996	0.459	0.409	$(1g_{9/2}, 1f_{5/2})_\nu$	0.974	0.929	0.889
	58	$(1f_{5/2}, 2p_{1/2})_\nu$	0.999	0.899	0.785	$(1g_{9/2}, 1f_{5/2})_\nu$	0.950	0.935	0.826
	60				$(1g_{9/2}, 1f_{5/2})_\nu$	0.936	0.936	0.936	
	62				$(1g_{9/2}, 1f_{5/2})_\nu$	0.946	0.935	0.931	
N = 20	30	$(2s_{1/2}, 1d_{5/2})_\pi$	0.950	0.865	0.722	$(1d_{5/2}, 1p_{1/2})_\pi$	0.543	0.395	0.364
	32	$(2s_{1/2}, 1d_{5/2})_\pi$	0.938	0.907	0.868	$(1d_{5/2}, 1p_{1/2})_\pi$	0.821	0.859	0.801
	34	$(2s_{1/2}, 1d_{5/2})_\pi$	0.925	0.923	0.921				
	36	$(1d_{3/2}, 2s_{1/2})_\pi$	1.003	0.903	0.827				
	38	$(1d_{3/2}, 2s_{1/2})_\pi$	0.999	0.808	0.659	$(1f_{7/2}, 1d_{3/2})_\pi$	0.520	0.824	0.806
	40				$(1f_{7/2}, 1d_{3/2})_\pi$	0.542	0.542	0.542	
	42	$(2p_{3/2}, 1f_{7/2})_\pi$	0.990	0.982	0.962	$(1f_{7/2}, 1d_{3/2})_\pi$	0.425	0.641	0.626
	44	$(2p_{3/2}, 1f_{7/2})_\pi$	0.977	0.958	0.938	$(1f_{7/2}, 1d_{3/2})_\pi$	0.420	0.831	0.806
	46	$(2p_{3/2}, 1f_{7/2})_\pi$	0.966	0.926	0.922	$(1f_{7/2}, 1d_{3/2})_\pi$	0.405	0.945	0.925

Table III: Values of  $\mathcal{W}(\mu\mu'; J^\Pi)$ , defined in Eq. (24), for the  $2^+$  and  $2^-$  states obtained in RPA, QRPA(F) and QRPA calculations. The subscripts  $\pi$  and  $\nu$  indicate proton and neutron configurations, respectively.

### C. Collectivity of the excited states

We have investigated how the pairing modifies the structure of the wave function of the excited states and, specifically, its degree of collectivity. To do this we have chosen quasi-particle pair configurations  $(\mu\mu')$  nearby the Fermi level where pairing effects are more important. In closed shell nuclei we have considered the pair formed by the HF s.p. states just below and above the Fermi surface. In open shell nuclei we studied the pairs involving the HF partially occupied s.p. state and either the first empty or the last fully occupied level. Neutron (proton) quasi-particle pair configurations were selected for  $Z = 8$  and  $Z = 20$  ( $N = 20$ ) chains. For each nucleus and multipolarity  $J^\Pi$  we have selected the excited states having as dominant configuration the quasi-particle pairs chosen and we have calculated the quantity

$$\mathcal{W}(\mu\mu'; J^\Pi) = [X_{\mu\mu'}(J^\Pi)]^* X_{\mu\mu'}(J^\Pi) - [Y_{\mu\mu'}(J^\Pi)]^* Y_{\mu\mu'}(J^\Pi). \quad (24)$$

Here  $X_{\mu\mu'}$  and  $Y_{\mu\mu'}$  are the (Q)RPA amplitudes of the quasi-particle pair, normalized as indicated in Eq. (5). We have followed the evolution of this quantity in the three types of calculations performed. Obviously, if  $\mathcal{W}(\mu\mu'; J^\Pi) \simeq 1$  the excited state is almost a pure quasi-particle pair configuration, while if the value is remarkably smaller than 1, then, contributions of other pairs appear and the nuclear excited state is more collective.

The most clear situations are those obtained for the  $2^+$  and  $2^-$  excitations whose results are shown in Table III. The values of  $\mathcal{W}(\mu\mu'; J^\Pi)$  in RPA results for the  $2^+$  excitations are very close to 1, and the inclusion of the pairing diminishes their values. This indicates that the pairing generates more collectivity. The opposite effect is present in the  $2^-$  excitation. For other multipoles the situation is more confused and each state has to be investigated individually.

### D. Pigmy dipole resonance

We have analyzed the low-lying isoscalar  $1^-$  excitation known in the literature as pigmy dipole resonance (PDR). Our results show the features already identified in RPA [35] and QRPA [14] calculations with Gogny interactions: the strength of the PDR increases with the neutron excess. On the other hand, the comparison between the results obtained with the three different type of calculations carried out in the present work indicates that the pairing effects are rather small.

In Fig. 4 we present the results obtained for the  $^{20}\text{O}$  and  $^{50}\text{Ca}$  nuclei, where the pairing generates the largest energy differences between the PDR states. The energy distributions of the  $B(E1)$  values are shown in the panels (a) and (d), the proton transition densities in the panels (b) and (e), and the neutron transition densities in the panels (c) and (f). The only remarkable effect of the pairing is in the neutron transition density of  $^{20}\text{O}$ , panel (c). In this case, the PDR excitation is dominated by the  $(1f_{7/2}, 1d_{5/2})_\nu$  quasi-particle pair. We use the subscripts  $\pi$  and  $\nu$  to indicate proton and neutron configurations, respectively. In the RPA case there are also remarkable contributions of other configurations,  $(1f_{5/2}, 1d_{5/2})_\nu$ ,  $(2f_{7/2}, 1d_{5/2})_\nu$  and  $(1d_{5/2}, 1p_{3/2})_\nu$ , but in QRPA only the latter configuration contaminates the dominant one. In any case, the global effect of the pairing is rather small.

### E. Conjugate configurations

We have already pointed out that in Fig. 2 we have considered those low-lying states which are well identified in RPA and the corresponding states obtained in QRPA(F) and QRPA calculations. In both QRPA(F) and QRPA, other low-energy excited states appear dominated by a quasi-particle configuration implying a s.p. transition between a partially occupied state and itself. We call *conjugate* these configurations. They play an important role in these calculations where the pairing interaction is active. However, in RPA they generate spurious excited states with energy nearby zero, and give a very small contribution in the wave functions of the other excited states.

In Fig. 5 we present energies (left panels) and  $B(E2)$  values (right panels) of the lowest QRPA(F) and QRPA  $2^+$  states, most of them dominated by conjugate configurations. Our results, indicated by the solid circles and triangles, are compared to the experimental data (solid squares) obtained from Ref. [36], with the exception of the  $B(E2)$  value of  $^{30}\text{Ne}$  which was measured more recently [9]. As first general remark, we observe that all the QRPA(F) energies are larger than those obtained in QRPA calculations. This is the same trend seen in Fig. 2.

In our calculations, the  $2^+$  excited states of the oxygen isotopes, whose energies and  $B(E2)$  values are shown in Figs. 5(a) and 5(d), are all dominated by the conjugate  $(1d_{5/2}, 1d_{5/2})_\nu$  configuration, with the exception of the  $^{24}\text{O}$  nucleus. The neutron  $1d_{5/2}$  state is completely full in  $^{22}\text{O}$  and  $^{24}\text{O}$ , but while in the first nucleus the  $(2s_{1/2}, 1d_{5/2})_\nu$  configuration competes with the dominant conjugate one, in the second nucleus the  $2^+$  excitation is dominated by

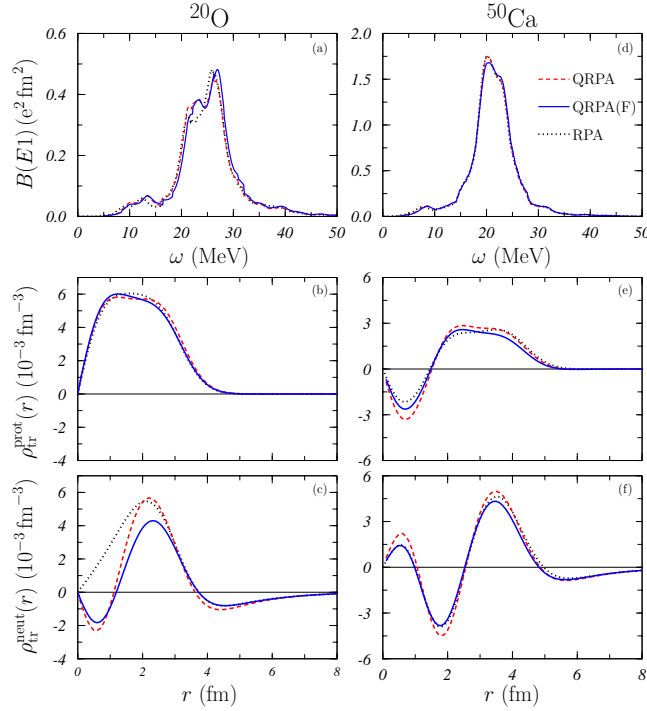


Figure 4: Energy distributions of the  $B(E1)$  values and transition densities for the states identified as PDR in  $^{20}\text{O}$  (left panels) and  $^{50}\text{Ca}$  (right panels). In all panels, red, blue and black curves indicate QRPA, QRPA(F) and RPA results, respectively. The  $B(E1)$  values energy distributions, shown in panels (a) and (d), have been obtained by folding the results of our calculations with a Lorentz function with 3 MeV width. Panels (b) and (e) show the proton transition densities, while panels (c) and (f) the neutron ones. In  $^{20}\text{O}$  ( $^{50}\text{Ca}$ ) these transition densities have been calculated for the states with excitation energies of 13.2 (8.6), 13.4 (8.6) and 12.4 (7.9) MeV, for QRPA, QRPA(F) and RPA, respectively.

the  $(1d_{3/2}, 2s_{1/2})_\nu$  configuration. The results of Ref. [13] are closer to our QRPA(F) energies than to those of the QRPA.

In the two panels, the open squares represent the results of the non-relativistic HFB+QRPA calculations of Ref. [8], which have been carried out by using the Skyrme interaction SLy4 [37] and a zero-range density-dependent interaction pairing force. The agreement between our results and those of Ref. [8] is good, certainly more satisfactory than the description of the experimental data. In this respect we do not observe any general trend and each case should be separately discussed.

We found that also the results of the relativistic calculations of Refs. [15, 16] show behaviors analogous to ours. The relativistic approach without dynamical pairing, which should correspond to our QRPA(F), generates excitation energies larger than those of the RPA. The inclusion of the pairing in the full relativistic QRPA reduces the values of these energies, as it happens in our calculations.

The results regarding the calcium isotopes are shown in the Figs. 5(b) and 5(e). Up to the  $^{48}\text{Ca}$  isotope, the  $2^+$  states are also dominated by a conjugate configuration, specifically the  $(1f_{7/2}, 1f_{7/2})_\nu$ . In  $^{48}\text{Ca}$  the neutron  $1f_{7/2}$  state is fully occupied and the excited state is dominated by the  $(2p_{3/2}, 1f_{7/2})_\nu$  pair. In the case of the heavier  $^{50}\text{Ca}$  isotope, the  $(2p_{3/2}, 2p_{3/2})_\nu$  conjugate configuration gives the main contribution to the lowest  $2^+$  state. On the other hand, in  $^{52}\text{Ca}$ , where the  $2p_{3/2}$  neutron state is fully occupied, the excited state is dominated by the  $(2p_{1/2}, 2p_{3/2})_\nu$  pair.

In Figs. 5(b) and 5(e) the open squares and circles represent the results of Refs. [11] and [12] respectively. The former have been obtained in HFB+QRPA non-relativistic calculations which used the SkM\* parameterization [38] of the Skyrme interaction and a separable Gaussian interaction as pairing force. The calculations of Ref. [12] considered the SLy5 Skyrme interaction [37] and a zero-range density-dependent pairing force.

Our results are in agreement with those of Ref. [11] in both energy and  $B(E2)$  values, with the exception of the  $^{40}\text{Ca}$  nucleus which we shall discuss below. We predict excitation energies larger than those experimentally found, except for  $^{52}\text{Ca}$  and  $^{54}\text{Ca}$ , and  $B(E2)$  values smaller than the observed ones, except for  $^{48}\text{Ca}$ . The calculations of Ref. [12] generate smaller values of the excitation energies and very large  $B(E2)$  values, even larger than those measured.

The  $2^+$  state of  $^{40}\text{Ca}$  in Ref. [11] is found at an energy much lower than that we have obtained (see panel (b) of

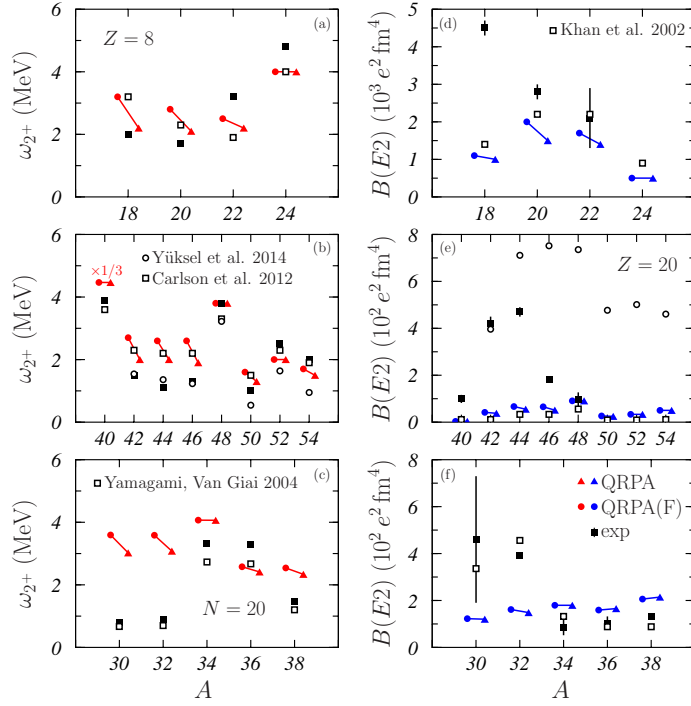


Figure 5: Energies (left panels) and  $B$ -values (right panels) of the lowest  $2^+$  excitations for some of the nuclei studied with  $Z = 8$  (panels (a) and (d)),  $Z = 20$  (panels (b) and (e)) and  $N = 20$  (panels (c) and (f)). The solid circles and triangles show our QRPA(F) and QRPA results, respectively. The solid squares indicate the experimental data from the compilation of Ref. [36], with the exception of the  $B(E2)$  value of  $^{30}\text{Ne}$  taken from Ref. [9]. The open squares represent the results of Khan et al. [8], for  $Z = 8$ , Carlson et al. [11], for  $Z = 20$ , and Yamagami and Van Giai [9], for  $N = 20$ . The open circles show the results of Yüksel et al. [12] also for  $Z = 20$ . Our QRPA and QRPA(F) energy values for the  $^{40}\text{Ca}$  nucleus are divided by a factor 3.

Fig. 5), but the authors of this article suggest the possibility that this  $2^+$  is a spurious state with a wrong number of nucleons.

The results found for the  $N = 20$  isotones are shown in the Figs. (c) and (f), where the open squares represent the values calculated in Ref. [9] by using the SkM\* interaction [38] plus a zero-range density-dependent interaction pairing force. The lowest  $2^+$  states of the  $^{34}\text{Si}$ ,  $^{36}\text{S}$  and  $^{38}\text{Ar}$  nuclei are dominated by the  $(2s_{1/2}, 1d_{5/2})_\pi$ , the  $(1d_{3/2}, 2s_{1/2})_\pi$  and the conjugate  $(1d_{3/2}, 1d_{3/2})_\pi$  pairs, respectively. For these nuclei, our results describe reasonably well the experimental data. However, the discrepancies for the  $^{30}\text{Ne}$  and  $^{32}\text{Mg}$  excitations, dominated by the conjugate  $(1d_{5/2}, 1d_{5/2})_\pi$  pair, are remarkable. By using a strong pairing interaction the results of Ref. [9] are able to reproduce the small experimental energies and the large  $B(E2)$  values.

## F. Magnetic dipole excitation

In the  $1^+$  excitations, the main part of the strength is concentrated in one excited state, which is dominated by a single quasi-particle pair. These dominant quasi-particle configurations are well identified, they are the  $(1d_{3/2}, 1d_{5/2})_\nu$  for the oxygen isotopes, the  $(1f_{5/2}, 1f_{7/2})_\nu$  for the calcium chain, and the  $(1d_{3/2}, 1d_{5/2})_\pi$  for the  $N = 20$  isotones up to  $Z = 20$ , and the  $(1f_{5/2}, 1f_{7/2})_\pi$  for the heavier ones. We show in panel (a) of Fig. 6 the energies of the  $1^+$  states with the largest  $B(M1)$  values for all the nuclei we have considered. The meaning of the symbols is the same as in Fig. 2. The available experimental values, taken from the compilation of Ref. [34], are shown by the open squares. The effects of the pairing on these energy values are certainly smaller than the differences with the experimental data.

In the panel (b) of Fig. 6 we represent the  $B(M1)$  values of these states. We observe that for each group of nuclei they increase up to a maximum corresponding to the doubly magic nucleus, and then they decrease. This behavior is related to the occupation  $v^2$  of the states involved. If we consider, for example, the calcium isotope chain, in the  $^{40}\text{Ca}$  nucleus the two s.p. states forming the  $(1f_{5/2}, 1f_{7/2})_\nu$  configuration are empty. The neutron  $1f_{7/2}$  state is partially occupied in  $^{42}\text{Ca}$  and its occupation progressively increases until it reaches full occupancy in  $^{48}\text{Ca}$ , where  $B(M1)$  is maximum. In all these isotopes the neutron  $1f_{5/2}$  state is empty. In  $^{50}\text{Ca}$ ,  $^{52}\text{Ca}$ , and  $^{54}\text{Ca}$  the  $B(M1)$  values remain almost stable because, in these isotopes, the additional neutrons occupy the  $2p_{3/2}$  s.p. state and, in the latter nucleus, also the  $2p_{1/2}$ , therefore the main neutron configuration is not affected. The  $B(M1)$  value reduces for the heavier

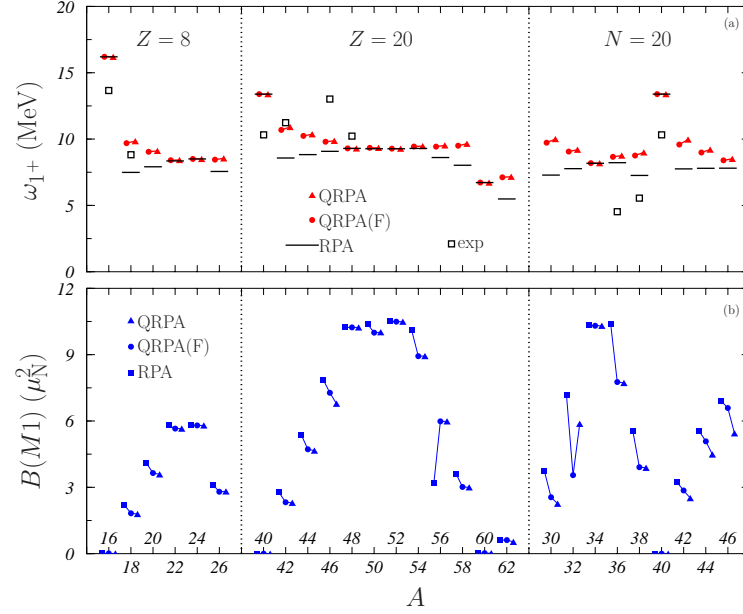


Figure 6: Energies, panel (a), and  $B(M1)$  values, panel (b), of the  $1^+$  states for all the nuclei we have studied. For each nucleus, we selected the  $1^+$  state with largest  $B(M1)$  value. The results of the QRPA(F) and QRPA calculations are shown by the solid circles and triangles, respectively. The RPA results are indicated by horizontal lines in panel (a) and by solid squares in panel (b). The open squares in panel (a) show the experimental values taken from the compilation of Ref. [34].

isotopes since the neutron  $1f_{5/2}$  state begins to be occupied and this diminishes the probability of the transition. This trend continues up to  $^{60}\text{Ca}$  where the  $1f_{5/2}$  s.p. state is fully occupied and the configuration  $(1f_{5/2}, 1f_{7/2})_\nu$  is not any more available.

The effect we have described has a remarkable experimental evidence in the electron scattering experiments of Ref. [39] even though, to the best of our knowledge, the small strength found in  $^{44}\text{Ca}$  with respect to the theoretical expectations remains unexplained.

We verified the validity of our interpretation of the  $B(M1)$  behavior by considering the quantity

$$R_B = \frac{1}{(u_\mu^{\text{HF}})^2 (v_{\mu'}^{\text{HF}})^2} \frac{B(M1)}{B(M1)_{\text{cs}}}, \quad (25)$$

where  $B(M1)_{\text{cs}}$  indicates the  $B(M1)$  value of a closed shell nucleus in each chain, specifically  $^{24}\text{O}$ ,  $^{48}\text{Ca}$  and  $^{34}\text{Si}$ , and  $(u_\mu^{\text{HF}})^2$  and  $(v_{\mu'}^{\text{HF}})^2$  are the HF occupation probabilities of the quasi-particles involved in the dominant configuration above mentioned. In the limiting case where the  $1^+$  state is composed only by the  $(\mu\mu')$  quasi-particle configuration, and the pairing is switched off,  $R_B$  is equal to unity. In this case, the behavior of the  $B(M1)$  values follows that of

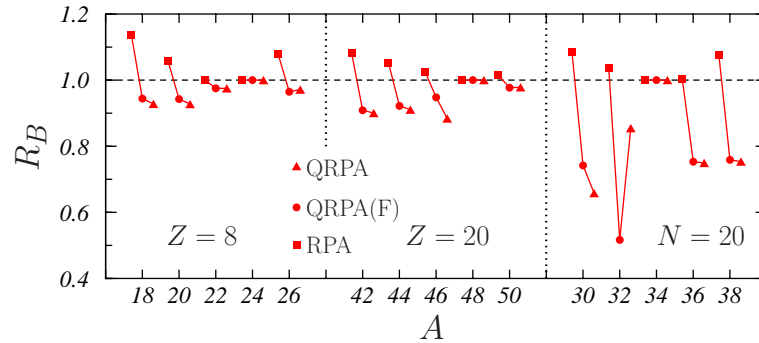


Figure 7: Values of  $R_B$ , as defined by Eq. (25), for those nuclei where in the main configurations forming the  $1^+$  states, i.e.  $(1d_{3/2}, 1d_{5/2})_\nu$  and  $(1f_{5/2}, 1f_{7/2})_\nu$  for oxygen and calcium isotopes, respectively, and  $(1d_{3/2}, 1d_{5/2})_\pi$  for the  $N = 20$  isotones, one of the s.p. states is partially occupied.

the corresponding HF occupation probabilities.

We show in Fig. 7 the  $R_B$  values for those nuclei where the configurations we are studying are active. The results are located around the unity within a 10% confirming our interpretation and indicating that pairing effects are negligible. The only exceptions are those of  $^{30}\text{Ne}$  and  $^{32}\text{Mg}$  nuclei. In the former case the large difference is due to the mixing of the main proton configuration with the  $(3s_{1/2}, 2s_{1/2})_\nu$  component. In the case of the  $^{32}\text{Mg}$  the main pair is mixed with the  $(3s_{1/2}, 1d_{3/2})_\nu$  configuration in the QRPA(F) calculations and this produces a separation of the  $1^+$  strength in two peaks. The inclusion of the  $G$  terms partially removes this mixing almost recovering the RPA result. In both cases the mixing of the main configuration with another one is due to small changes of the s.p. energies which generate s.p. transitions with very similar energies.

### G. Giant resonances

We have presented so far the effects of the pairing on the low-lying excitations, and now we discuss the giant resonance region where the main part of the strength is concentrated. We summarize the large information regarding this energy region by considering the centroid energies:

$$\omega_{\text{centr}} = \frac{\sum_{\omega=\omega_{\text{min}}}^{\omega_{\text{max}}} \omega B(\omega, 0^+ \rightarrow J^\Pi)}{\sum_{\omega=\omega_{\text{min}}}^{\omega_{\text{max}}} B(\omega, 0^+ \rightarrow J^\Pi)}. \quad (26)$$

Here we have used  $\omega_{\text{min}} = 0$  for all the multipoles with the exception of the  $2^+$ , where we have considered  $\omega_{\text{min}} = 10$  MeV to eliminate the large contribution of the low-lying states dominated by conjugate configurations. The sums extend up to  $\omega_{\text{max}} = 80$  MeV in all cases. The multipoles  $1^-$ , where we excluded the spurious states,  $2^\pm$  and  $3^\pm$  have been considered. We did not calculate the centroids for the  $1^+$  states because their strengths are concentrated

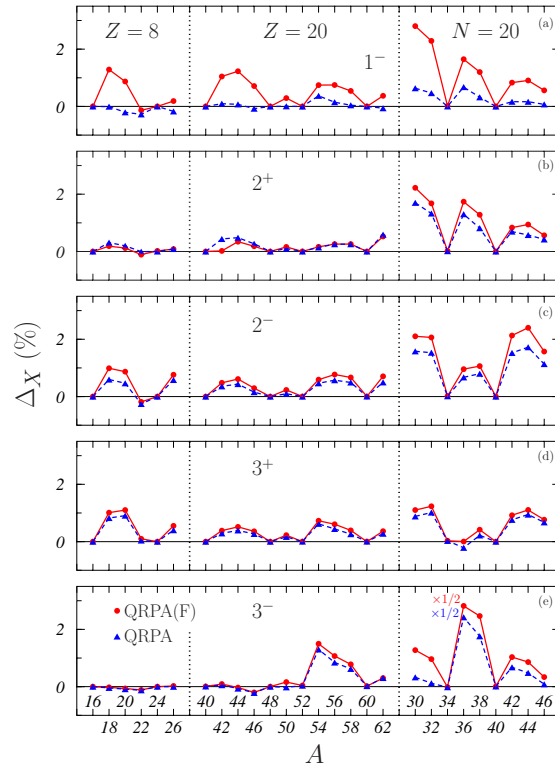


Figure 8: Relative differences  $\Delta_X$  in percentage, as defined in Eq. (27), for  $1^-$ ,  $2^\pm$ , and  $3^\pm$  multipoles of the various nuclei investigated. Solid circles and triangles indicate QRPA(F) and QRPA results, respectively. The values of the  $3^-$  excitation in  $^{36}\text{S}$  have been divided by 2.

in a single state as we have already mentioned. The consistency of our calculations have been tested by verifying the exhaustion of the Thomas-Reiche-Khun and the isoscalar sum rules [40]. We obtained results analogous to those found in RPA calculations [32, 35]. More details are given in Appendix A.

In Fig. 8 we show the relative differences

$$\Delta_X = \frac{\omega_{\text{centr}}^X - \omega_{\text{centr}}^{\text{RPA}}}{\omega_{\text{centr}}^X + \omega_{\text{centr}}^{\text{RPA}}}, \quad (27)$$

with  $X \equiv \text{QRPA(F)}$  and QRPA. The solid circles indicate the QRPA(F) results and the triangles those of the QRPA calculations. Except in a few cases, these relative differences are positive, indicating that the pairing is enhancing the position of the centroid. In almost all nuclei and multipolarities, the differences are larger in QRPA(F) than in QRPA. The largest effect is seen for the  $N = 20$  isotones and the largest differences between QRPA(F) and QRPA calculations are found for the  $1^-$  multipolarity.

## V. SUMMARY AND CONCLUSIONS

We have investigated the excitation spectrum of 6 oxygen isotopes, 12 calcium isotopes and 9 isotones with  $N = 20$  by using a HF+BCS+QRPA approach with the aim of studying global effects of the pairing. We have used the same effective nucleon-nucleon force for the HF part of our calculations, for the pairing sector, and as residual interaction in QRPA. We presented results obtained by using the D1M parameterization of the Gogny force [26]. In our approach, pairing effects enter in the construction of the s.p. configuration space generated by the HF+BCS calculations, and in the results of the QRPA where, in presence of pairing, the  $G$  terms of Eqs. (11) and (12) become active. We carried out calculations that we labelled RPA by using HF s.p. states and without  $G$  terms, and also calculations with HF+BCS s.p. states but without  $G$  terms, that we called QRPA(F). The comparison between RPA, QRPA(F) and full HF+BCS+QRPA calculations, that we called QRPA, has been used to disentangle the source of the pairing effects. We summarize here below the main results of our study.

- The s.p. wave functions, occupation probabilities and energies, together with the effective nucleon-nucleon interaction are the input of the QRPA calculations. The pairing effects on this input are related to the modifications of the s.p. energies and of the occupation probabilities with respect to the HF values. We found a poor correlation between the effects of the pairing on these two quantities. In other words, our results show that large modifications of the occupation probabilities do not imply large modifications of the s.p. energies, and viceversa (see Fig. 1).
- We observed that, in general, QRPA(F) and QRPA energies are larger than those obtained in RPA calculations. We also found that, for each excited state, the QRPA(F) energies are larger than those of the QRPA. The differences between QRPA(F) and QRPA energies are smaller than those with the RPA. We concluded that the pairing effect on the s.p. input produces an increase of the excitation energies, while in the QRPA calculations it acts in the opposite direction. The former effect is larger than that of the other one such as the final results is that QRPA energies are still larger than those of the RPA (see Figs. 2 and 3).
- While the effects of the pairing on the excitation energy are well identified and have a common trend, those concerning the changes on the many-body wave functions are more difficult to single out and describe. We have defined an index  $\mathcal{W}(\mu\mu'; J^\Pi)$ , Eq. (24), to quantify the degree of collectivity of an excited state. We found general trends only in quadrupole excitations where our results indicate that the pairing increases the collectivity of the  $2^+$  states while it reduces that of the  $2^-$  states (see Table III).
- We have observed that pairing effects on the  $1^-$  excitation, especially on the PDR, are negligible (see Fig. 4).
- The study of the first excited  $2^+$  states dominated by conjugate transitions allows a comparison with other calculations and shows that our pairing effects are relatively small (see Fig. 5).
- The strength of the  $1^+$  excitation is concentrated on a single state, but we did not find remarkable global pairing effects. Specific cases deserve a more thorough investigation (see Figs. 6 and 7).
- The study of the excitations in the giant resonance region indicates that the energies of the giant resonance centroids increase when the pairing is included (see Fig. 8).

The description of the experimental data for the excited states and nuclei studied does not significantly improve if pairing is taken into account. In general, the pairing effects are smaller than the discrepancy with the experimental



s.p. state	HF	HF+BCS			HFB		
	$\epsilon_\mu$	$v_\mu^2$	$E_\mu$	$\tilde{\epsilon}_\mu$	$v_\mu^2$	$E_\mu$	$\epsilon_\mu$
$1s_{1/2}$	-36.73	0.999	30.35	-36.78	0.998	30.37	-36.88
$1p_{3/2}$	-19.95	0.995	13.65	-20.08	0.991	14.31	-20.66
$1p_{1/2}$	-15.79	0.991	9.53	-15.96	0.983	9.39	-15.72
$1d_{5/2}$	-5.88	0.332	1.63	-4.80	0.323	2.25	-5.81
$2s_{1/2}$	-2.68	0.010	3.83	-2.60	0.025	4.28	-1.98
$1d_{3/2}$	1.16	0.004	7.65	1.22	0.011	8.24	2.77

Table IV: Occupation probabilities and energies of the neutron quasi-particle states obtained in HF, HF+BCS and HFB calculations for neutron states in  $^{18}\text{O}$  with  $v^2 < 10^{-4}$ . The HF energies  $\epsilon_\mu$ , the quasi-particle energies  $E_\mu$ , defined in Eq. (1), and the energies  $\tilde{\epsilon}_\mu$ , defined in Eq. (21), are expressed in MeV.

data. We cannot exclude the possibility that a different parameterization of the effective nucleon-nucleon interaction, with the same fitting qualities of the Gogny force, can produce larger pairing effects and a better description of the experimental data. However, we think more probable that these discrepancies are due to physical phenomena that the HF+BCS+QRPA approach cannot describe.

### Appendix A: Results for $^{18}\text{O}$

In this appendix we discuss some details regarding the convergence of our HF+BCS+QRPA calculations. As example we present the results obtained for the  $^{18}\text{O}$  nucleus. We conducted analogous tests for the heavier nuclei we have considered in our investigation and we obtained similar results.

We carried out HF and BCS calculations by using a box integration radius of 12 fm. We obtained binding energies of 136.54 MeV in HF and 138.92 MeV in HF+BCS, to be compared with the experimental value of 139.8 MeV [34]. The value obtained by carrying out a HFB calculation with the approach developed in [41] is 139.8 MeV.

In Table IV we give the HF energies  $\epsilon_\mu$ , the occupation probabilities  $v_\mu^2$ , the quasi particle energies  $E_\mu$ , and the BCS s.p. energies  $\tilde{\epsilon}_\mu$  for the neutron s.p. states with  $v_\mu^2 > 10^{-4}$ . For sake of completeness we give the values of the same quantities obtained in a HFB calculation.

The configuration space used in the QRPA calculations includes all the s.p. states with energy smaller than a chosen value  $E_p$ . We insert a further restriction regarding the number of quasi-particle pairs. We neglect those pairs composed by quasi-particles whose energy is, individually, larger than  $E_{pp}$ . This second restriction is useful in heavy nuclei, but, in the case of the nuclei studied in the present work, we have always used  $E_p = E_{pp}$ . Nevertheless, the use of these two cutoff energies is not enough to generate QRPA matrices of dimension smaller than 4000, which is our numerical limitation. The problem is generated by the large number of configuration pairs where both s.p. states have  $\epsilon_\mu > \lambda$ . For the excited states of our interest, i.e. the low-lying ones and the giant resonances, the contribution of many of these last type of pairs, is scarcely relevant. These are pairs where the wave functions describing both quasi-particle states are non-resonant and lying high in the continuum. For this reason we further reduce the number of this type of pairs by omitting those where the occupation probability  $v^2$  of both states forming the pair is smaller than a critical value  $v_{\text{cut}}^2$ .

As example, we show in Table V the excitation energies, and the corresponding  $B(E1)$  values, of the first two

calculation	$v_{\text{cut}}^2$	# of pairs	$1_1^-$		$1_2^-$	
			$\omega$ (MeV)	$B(E1)$ ( $e^2 \text{fm}^2$ )	$\omega$ (MeV)	$B(E1)$ ( $e^2 \text{fm}^2$ )
A	-	1112	2.73	$1.87 \cdot 10^{-3}$	10.62	$8.18 \cdot 10^{-2}$
B	$10^{-5}$	271	2.76	$1.86 \cdot 10^{-3}$	10.64	$7.73 \cdot 10^{-2}$
C	$10^{-3}$	164	2.79	$1.53 \cdot 10^{-3}$	10.65	$7.53 \cdot 10^{-2}$

Table V: Excitation energies and  $B(E1)$  values of the first two  $1^-$  states of  $^{18}\text{O}$  in the HF+BCS+QRPA approach. In all the cases we used  $E_p = E_{pp} = 100$  MeV. The results of calculation A have been obtained without any further limitation of the s.p. configuration space. In calculations B and C we have excluded those pairs where both quasi-particle states have  $v_\mu^2 < 10^{-5}$  and  $10^{-3}$ , respectively.

$E_p = E_{pp}$	$\omega_1$	$B_1(E1)$	$\omega_2$	$B_2(E1)$	$\omega_3$	$B_3(E1)$
60.0	3.22	$2.98 \cdot 10^{-3}$	11.16	$1.19 \cdot 10^{-2}$	11.99	$1.27 \cdot 10^{-1}$
80.0	3.11	$2.51 \cdot 10^{-3}$	11.12	$1.00 \cdot 10^{-2}$	11.98	$1.29 \cdot 10^{-1}$
100.0	2.68	$2.76 \cdot 10^{-3}$	11.02	$7.43 \cdot 10^{-3}$	11.96	$1.32 \cdot 10^{-1}$
120.0	2.55	$2.64 \cdot 10^{-3}$	10.98	$6.37 \cdot 10^{-3}$	11.95	$1.33 \cdot 10^{-1}$
140.0	2.41	$1.89 \cdot 10^{-3}$	10.96	$5.85 \cdot 10^{-3}$	11.94	$1.35 \cdot 10^{-1}$
160.0	2.16	$1.71 \cdot 10^{-3}$	10.94	$5.14 \cdot 10^{-3}$	11.94	$1.36 \cdot 10^{-1}$
180.0	2.12	$1.62 \cdot 10^{-3}$	10.93	$4.94 \cdot 10^{-3}$	11.93	$1.36 \cdot 10^{-1}$
200.0	1.92	$1.69 \cdot 10^{-3}$	10.92	$4.63 \cdot 10^{-3}$	11.93	$1.36 \cdot 10^{-1}$
250.0	1.87	$1.34 \cdot 10^{-3}$	10.91	$4.48 \cdot 10^{-3}$	11.93	$1.37 \cdot 10^{-1}$

Table VI: Excitation energies,  $\omega$  in MeV, and  $B(E1)$  values, in  $e^2 \text{ fm}^2$ , of the first three  $1^-$  excited states as a function of the cutoff energies  $E_p$  and  $E_{pp}$ , also expressed in MeV.

$1^-$  excited states. The  $1_1^-$  state is the spurious isoscalar excitation related to the centre of mass motion. All the calculations have been carried out with  $E_p = E_{pp} = 100 \text{ MeV}$ . The results of calculation A have been obtained without any further limitations of the s.p. configuration space, by handling 1112 pairs. We reduce this number by using  $v_{\text{cut}}^2 = 10^{-5}$  (calculation B), and  $v_{\text{cut}}^2 = 10^{-3}$  (calculation C). Even though there is a remarkable reduction of the number of pairs when the selection related to  $v_{\text{cut}}^2$  is activated, the energy eigenvalues are only modified by a few tens of keV. The  $B(E1)$  values are more sensitive to this reduction.

We tested the sensitivity of the energy of the spurious isoscalar  $1^-$  state to the dimensions of the configuration space. In Table VI we show energies and  $B$ -values of the first three  $1^-$  states obtained with  $v_{\text{cut}}^2 = 10^{-5}$ . We have carried out calculations by using different values of  $E_p = E_{pp}$ . It is evident that the spurious state is extremely sensitive to the size of the configuration space, while the energies of the other two states change very little.

We also checked the presence of a low-lying  $0^+$  spurious state generated by the non conservation of the particle number in the nuclear wave function. Also in this case the energy of this spurious state is extremely sensitive to the dimensions of the quasi-particle configuration space. When we used  $E_p = E_{pp} = 60 \text{ MeV}$  we found this  $0^+$  state at  $0.11 \text{ MeV}$ . With larger configuration spaces,  $E_p = E_{pp} > 100 \text{ MeV}$ , it is below zero and the QRPA secular equations (10) have an imaginary solution.

We tested the stability of our solutions by changing of 10% the  $E_p$  and  $E_{pp}$  values. In all cases we obtained differences in the QRPA energies within the numerical accuracy.

The results presented in this paper have been carried out by using the values  $E_p = E_{pp} = 200 \text{ MeV}$  and  $v_{\text{cut}}^2 = 10^{-3}$ , which ensure the stability of the results for all the nuclei studied, even in  $^{62}\text{Ca}$ , the heaviest one.

Finally, we evaluated energy weighted sum rules by integrating up to the excitation energy of  $50 \text{ MeV}$ , and using  $E_p = E_{pp} = 200 \text{ MeV}$ . For the  $1^-$  excitation we calculated the Thomas-Reiche-Kuhn sum rule which we found exhausted up to the 0.95 of the expected value, this last one calculated by considering an enhancement factor of  $\kappa = 0.5$  with respect to the traditional value [32, 42]). For the isoscalar  $0^+$  and  $1^-$  excitations [10, 40] we found an over estimation of the expected values of about 1.1, to be compared with the values of 0.86 and 0.96 obtained, respectively, when RPA calculations have been carried out. The source of this discrepancy is under investigation.

### Acknowledgments

This work has been partially supported by the Junta de Andalucía (FQM387), the Spanish Ministerio de Economía y Competitividad (FPA2015-67694-P) and the European Regional Development Fund (ERDF).

- 
- [1] A. Bohr, B. Mottelson, D. Pines, Phys. Rev. 110 (1958) 936.
  - [2] M. Baranger, Phys. Rev. 120 (1960) 957.
  - [3] M. Anguiano, A. M. Lallena, G. Co', V. De Donno, J. Phys. G 41 (2014) 025102.
  - [4] M. Anguiano, A. M. Lallena, G. Co', V. De Donno, J. Phys. G 42 (2015) 079501.
  - [5] M. Anguiano, R. N. Bernard, A. M. Lallena, G. Co', V. De Donno, Nucl. Phys. A 955 (2016) 181.
  - [6] J. Dechargé, D. Gogny, Phys. Rev. C 21 (1980) 1568.
  - [7] N. Paar, D. Vretenar, E. Khan, G. Colò, Rep. Prog. Phys. 70 (2007) 691.

- [8] E. Khan, N. Sandulescu, M. Grasso, N. Van Giai, Phys. Rev. C 66 (2002) 024309.
- [9] M. Yamagami, N. Van Giai, Phys. Rev. C 69 (2004) 034301.
- [10] J. Terasaki, J. Engel, M. Bender, J. Dobaczewski, W. Nazarewicz, M. Stoitsov, Phys. Rev. C 71 (2005) 034310.
- [11] B. G. Carlson, J. Toivanen, A. Pastore, Phys. Rev. C 86 (2012) 014307.
- [12] E. Yüksel, N. Van Giai, E. Khan, K. Bozkurt, Phys. Rev. C 89 (2014) 064322.
- [13] G. Giambrone, S. Scheit, F. Barranco, P. Bortignon, G. Colò, D. Sarchi, E. Vigezzi, Nucl. Phys. A 726 (2005) 3.
- [14] M. Martini, S. Péru, M. Dupuis, Phys. Rev. C 83 (2011) 034309.
- [15] N. Paar, P. Ring, T. Nikšić, D. Vretenar, Phys. Rev. C 67 (2003) 034312.
- [16] L.-G. Cao, Z.-Y. Ma, Phys. Rev. C 71 (2005) 034305.
- [17] S. Goriely, S. Hilaire, M. Girod, S. Péru, Phys. Rev. Lett. 102 (2009) 242501.
- [18] G. Co', A. M. Lallena, Nuovo Cimento A 111 (1998) 527.
- [19] P. Ring, P. Schuck, The nuclear many-body problem, Springer, Berlin, 1980.
- [20] J. Suhonen, From nucleons to nucleus, Springer, Berlin, 2007.
- [21] A. R. Edmonds, Angular momentum in quantum mechanics, Princeton University Press, Princeton, 1957.
- [22] F. Catara, N. Dinh Dang, M. Sambataro, Nucl. Phys. A 579 (1994) 1.
- [23] J. Schwieger, F. Simkovic, A. Faessler, Nucl. Phys. A 600 (1996) 179.
- [24] A. Mariano, J. G. Hirsch, Phys. Rev. C 57 (1998) 3015.
- [25] F. Chappert, Nouvelles paramétrisation de l'interaction nucléaire effective de Gogny, Ph.D. thesis, Université de Paris-Sud XI (France), <http://tel.archives-ouvertes.fr/tel-001777379/en/> (2007).
- [26] J. F. Berger, M. Girod, D. Gogny, Comp. Phys. Commun. 63 (1991) 365.
- [27] J. L. Egido, J. Lessing, V. Martin, L. M. Robledo, Nucl. Phys. A 594 (1995) 70.
- [28] V. De Donno, G. Co', M. Anguiano, A. M. Lallena, Phys. Rev. C 89 (2014) 014309.
- [29] A. R. Bautista, G. Co', A. M. Lallena, Nuovo Cimento A 112 (1999) 1117.
- [30] M. Anguiano, G. Co', V. De Donno, A. M. Lallena, Phys. Rev. C 83 (2011) 064306.
- [31] S. V. Tolokonnikov, S. Kamedzhiev, D. Voitenkov, S. Krewald, E. E. Saperstein, Phys. Rev. C 84 (2011) 064324.
- [32] V. De Donno, G. Co', M. Anguiano, A. M. Lallena, Phys. Rev. C 83 (2011) 044324.
- [33] M. Matsuo, K. Mizuyama, Y. Serizawa, Phys. Rev. C 71 (2005) 064326.
- [34] Brookhaven National Laboratory, National nuclear data center, <http://www.nndc.bnl.gov/>.
- [35] G. Co', V. De Donno, M. Anguiano, A. M. Lallena, Phys. Rev. C 87 (2013) 034305.
- [36] S. Raman, C. W. Nestor Jr., P. Tikkanen, Atomic Data and Nuclear Data Tables 78 (2001) 1.
- [37] E. Chabanat, P. Bonche, P. Haensel, J. Meyer, F. Schaeffer, Nucl. Phys. A 635 (1998) 231.
- [38] J. Bartel, P. Quentin, M. Brack, C. Guet, H. B. Håkansson, Nucl. Phys. A 386 (1982) 79.
- [39] W. Steffen, H.-D. Gräf, W. Gross, D. Meuer, A. Richter, E. Spamer, O. Titze, W. Knüpfer, Phys. Lett. B 95 (1980) 23.
- [40] M. N. Harakeh, A. van der Woude, Giant resonances, Clarendon press, Oxford, 2001.
- [41] M. Anguiano, J. L. Egido, L. M. Robledo, Nucl. Phys. A 683 (2001) 227.
- [42] H. Nakada, K. Mizuyama, M. Yamagami, M. Matsuo, Nucl. Phys. A 828 (2009) 283.